

Capacity-Approaching Polar Codes with Long Codewords and Successive Cancellation Decoding Based on Improved Gaussian Approximation

Hideki Ochiai, *Senior Member, IEEE*, Patrick Mitran, *Senior Member, IEEE*, and
H. Vincent Poor, *Fellow, IEEE*

Abstract

This paper focuses on an improved Gaussian approximation (GA) based construction of polar codes with successive cancellation (SC) decoding over an additive white Gaussian noise (AWGN) channel. It has been theoretically proven by Arkan that polar codes with low-complexity SC decoder can approach the channel capacity of an arbitrary symmetric binary-input discrete memoryless channel, provided that the code length is chosen large enough. Nevertheless, how to construct such codes over an AWGN channel with low computational effort has been an open problem. The conventional GA is a powerful and low complexity technique, but due to numerical issues, it can fail to accurately trace the evolution of the mean log likelihood ratio (LLR) value as the code length increases. In this work, an improved GA approach is proposed where, by judiciously defining the functions associated with the GA, an accurate trace of mean LLR evolution becomes feasible. With this improved GA, through theoretical analysis and simulations with code lengths up to $N = 2^{18}$, we explicitly demonstrate that various code-rate polar codes with long codeword and capacity approaching behavior can be easily constructed.

H. Ochiai is with the Department of Electrical and Computer Engineering, Yokohama National University, Yokohama, Japan.
email: hideki@ynu.ac.jp

P. Mitran is with the Department of Electrical and Computer Engineering, University of Waterloo, ON, Canada.
email: mitran@uwaterloo.ca

H. V. Poor is with the Department of Electrical Engineering, Princeton University, Princeton, NJ. email: poor@princeton.edu

Index Terms

Block error rate, code construction, density evolution, Gaussian approximation, polar codes.

I. INTRODUCTION

Polar codes, introduced by Arıkan [1], have the salient property that they can achieve channel capacity by low-complexity successive cancellation (SC) decoding. In order to approach the capacity over a practical additive white Gaussian noise (AWGN) channel by SC decoding, not only must the code length be large, but also the code structure must be properly designed. The difficulty of polar code design lies in the fact that polar codes with SC decoding are not universal [2]–[4] in the sense that codes that perform well in a low signal-to-noise power ratio (SNR) regime do not necessarily perform well in a higher SNR regime. Therefore, practical code design should be able to capture its performance for given operating SNR and code rate.

In the framework of polar codes, code construction is equivalent to the selection of information bit locations, referred to as the *information set* [1]. These are chosen from among all the input bits to the rate-1 polar encoder. Several approaches for polar code construction, i.e., algorithms for information set selection, have been developed in the literature for an AWGN channel. Mori and Tanaka [5] proposed the use of density evolution (DE), originally developed for the design of irregular low-density parity-check (LDPC) codes by Richardson *et al.* in [6]. Since directly tracing the density of log likelihood ratios (LLR) is computationally challenging, Tal and Vardy developed a practical approach for DE based on the concept of upgrading and degrading quantization [7]. The complexity depends on the quantization parameter, which should be carefully chosen considering the required accuracy.

Meanwhile, for design and analysis of LDPC codes, Chung *et al.* proposed the use of a Gaussian approximation (GA) [8]. Instead of tracing the exact density of the LLRs, GA only traces the mean, which is sufficient if the LLR is modeled as a Gaussian distribution. Trifonov [9] demonstrated that the GA can be also used for constructing polar codes with SC decoding. Subsequently, the effectiveness of the GA for polar code construction has also been confirmed in [10], [11]. Furthermore, in [11], [12], the use of the Bhattacharyya parameter [1] for information set selection, which is strictly valid only for the case of binary erasure channels, has been shown by simulation to be effective provided that the operating SNR parameter is appropriately chosen by an empirical approach.

In order for polar codes with SC decoding to outperform LDPC codes, it is known that the code length should be much larger than that of LDPC codes [13]. In other words, polar codes over an AWGN channel with moderate code length are not competitive with other capacity approaching codes. Since then, the use of conventional decoding approaches such as belief propagation (BP) decoding has also been studied [14]–[16]. On the other hand, Tal and Vardy showed that successive cancellation *list* (SCL) decoding improves the performance, and furthermore, the application of error detection codes such as cyclic redundancy-check (CRC) codes in combination with SCL decoding is shown to outperform other competitive codes [17]. Since then, most studies on polar codes target moderate block-length codes assuming more sophisticated decoding. As a consequence, studies for polar code construction have also pursued decoding specific designs such as those proposed in [18] and [19].

Here, we recall that a major advantage of polar codes as proposed by Arikan [1] is its simplicity of encoding and SC decoding with its capacity achieving performance. The only issue is that the code length should be much larger compared to LDPC codes [13] for the same or better target performance. Therefore, we are interested in constructing polar codes for SC decoding with very large code length and evaluating its performance over a practical AWGN channel with low complexity construction approach. The complexity of Tal and Vardy scheme [7] becomes non-negligible, and thus we focus on GA as a low-complexity alternative. The key idea of GA is to trace the mean value of the LLRs assuming that the LLRs follow a Gaussian distribution. Furthermore, if the mean is estimated accurately through GA, the block error rate (BLER) can be precisely estimated without resorting to simulations. In this work, we first elucidate the limitation of the conventional GA in its mean LLR estimation process, especially as the code length increases. It turns out that the straightforward implementation of conventional GA fails to construct good polar codes with capacity approaching behavior at large block length (as will be illustrated in Fig. 5 in Section V-B). This stems from the fact that the dynamic range of the LLR values increases exponentially with code length, and thus the conventional approach cannot accurately trace the evolution of mean LLR values. We then propose a solution to this numerical issue by carefully studying the behavior of specific functions involved in GA. With this proposed approach, which we refer to as an *improved GA*, we can easily estimate the performance of polar codes with SC decoding for long codes with low complexity. We then demonstrate simulation results with block length $N = 2^{18}$ and show that the results perfectly match with the estimated

BLER results obtained by the analysis using the improved GA.

We also investigate another construction scheme based on the flipping probability of an LLR. Similar to the case of GA, this approach can accurately estimate the BLER without simulation. By tracing the flipping probability instead of its mean value, it is still possible to construct the codes with large code length, even though numerical results show its sub-optimality over the improved GA as the code length increases.

The major contributions of this paper are summarized as follows:

- An improved GA method that can trace the evolution of LLRs over an AWGN channel with precise numerical accuracy is proposed. This is necessary for constructing large block-length polar codes with almost negligible complexity.
- The capacity-approaching behavior of the polar codes designed by the proposed GA with low-complexity SC decoding is demonstrated by Monte-Carlo simulation. This demonstration is performed with block-lengths as large as $N = 2^{18}$ and includes a corresponding analysis based on the estimated BLER.
- The effectiveness of the proposed GA is confirmed through comparison with the other low-complexity construction approaches.
- Through the theoretical analysis, we elucidate the accuracy and possible limitations of GA in the case of low SNR regime.

This paper is organized as follows. Section II introduces notations associated with the polar codes and decoding used throughout this work. The construction based on GA using the proposed calculation approach is presented in Section III. As an alternative and tractable approach to GA, a construction based on LLR flipping probability is described in Section IV. Numerical examples are given in Section V, where the capacity-approaching behavior based on the construction using the improved GA is demonstrated. Finally, Section VI concludes this work.

II. POLAR CODES AND SUCCESSIVE CANCELLATION DECODING

A. Polar Code

Let $\mathbf{u} = (u_0, u_1, \dots, u_{N-1}) \in \mathbb{F}_2^N$ denote a binary input vector of length N . Let $\mathbf{G}_N \in \mathbb{F}_2^{N \times N}$ denote a generator matrix formulated as

$$\mathbf{G}_N = \mathbf{G}_2^{\otimes n}, \quad \mathbf{G}_2 = \begin{pmatrix} 1 & 0 \\ 1 & 1 \end{pmatrix}, \quad (1)$$

where $n = \log_2 N$ and $\mathbf{A}^{\otimes n} = \mathbf{A} \otimes \mathbf{A}^{\otimes (n-1)}$ is the n th Kronecker power of matrix \mathbf{A} with $\mathbf{A}^{\otimes 0} = (1)$ [1]. The corresponding output $\mathbf{x} = (x_0, x_1, \dots, x_{N-1}) \in \mathbb{F}_2^N$ is expressed as

$$\mathbf{x} = \mathbf{u} \mathbf{B}_N \mathbf{G}_N, \quad (2)$$

where $\mathbf{B}_N \in \mathbb{F}_2^{N \times N}$ is the $N \times N$ bit reversal permutation matrix [1] which guarantees that SC decoding is performed in the bit reversal order of the binary channel index.

We assume BPSK modulation over an AWGN channel, i.e., the transmitted symbol $s_i \in \mathbb{R}$, $i = 0, 1, \dots, N-1$, is given by

$$s_i = \sqrt{E_s}(1 - 2x_i), \quad (3)$$

with E_s representing the symbol energy, and the received symbol $y_i \in \mathbb{R}$ is

$$y_i = s_i + z_i, \quad (4)$$

where $z_i \sim \mathcal{N}(0, N_0/2)$, i.e., z_i is a real-valued Gaussian random variable with zero mean and variance $N_0/2$. We denote the received signal vector of length $N = 2^n$ as $\mathbf{y}_n = (y_0, y_1, \dots, y_{2^n-1})$, and its subvector of length 2^m starting from the index i as $\mathbf{y}_m^{(i)} = (y_i, y_{i+1}, \dots, y_{i+2^m-1})$.

B. Successive Cancellation Decoding

Based on SC decoding, given the length- 2^n received symbol observation vector \mathbf{y}_n , each input bit u_i , $i = 0, 1, \dots, N-1$, is decoded based on its corresponding LLR. We use the following short-hand notation for LLR of the i th input bit u_i as

$$L_n^{(i)}(\mathbf{y}_n) = \begin{cases} \log \frac{\Pr(\mathbf{y}_n | u_i=0)}{\Pr(\mathbf{y}_n | u_i=1)}, & i = 0, \\ \log \frac{\Pr(\mathbf{y}_n, \hat{\mathbf{u}}_{i-1} | u_i=0)}{\Pr(\mathbf{y}_n, \hat{\mathbf{u}}_{i-1} | u_i=1)}, & i = 1, 2, \dots, 2^n - 1, \end{cases} \quad (5)$$

where $\hat{\mathbf{u}}_{i-1} = (\hat{u}_0, \hat{u}_1, \dots, \hat{u}_{i-1})$ is the vector containing the estimated bits that have been already determined upon decoding of the i th bit. (The subscript n of $L_n^{(i)}$ reflects the fact that the LLR is calculated based on the observation of 2^n received symbols in addition to the previously estimated input bits.) Note that for simplicity of notation, we will omit the dependence of LLR on the previously estimated bits $\hat{\mathbf{u}}_{i-1}$ in what follows.

Because of the unique structure of polar codes, the above LLRs can be recursively calculated for $k = 1, 2, \dots, n$ with $n = \log_2 N$ and $i = 0, 1, \dots, 2^{k-1} - 1$ as [1], [5]

$$L_k^{(2i)}(\mathbf{y}_k) = L_{k-1}^{(i)}(\mathbf{y}_{k-1}^{(0)}) \boxplus L_{k-1}^{(i)}(\mathbf{y}_{k-1}^{(2^{k-1})}) \quad (6)$$

$$L_k^{(2i+1)}(\mathbf{y}_k) = L_{k-1}^{(i)}(\mathbf{y}_{k-1}^{(2^{k-1})}) + (-1)^{\hat{u}_{2i}} L_{k-1}^{(i)}(\mathbf{y}_{k-1}^{(0)}), \quad (7)$$

or by rewriting $L_k^{(2i)} \triangleq L_k^{(2i)}(\mathbf{y}_k)$, $L_{k-1}^{(i)} \triangleq L_{k-1}^{(i)}(\mathbf{y}_{k-1}^{(0)})$, and $L_{k-1}^{(i)'} \triangleq L_{k-1}^{(i)}(\mathbf{y}_{k-1}^{(2^{k-1})})$ for simplicity, we have

$$L_k^{(2i)} = L_{k-1}^{(i)} \boxplus L_{k-1}^{(i)'} \quad (8)$$

$$L_k^{(2i+1)} = L_{k-1}^{(i)'} + (-1)^{\hat{u}_{2i}} L_{k-1}^{(i)}. \quad (9)$$

As noted in [5], (8) corresponds to the LLR calculation associated with a check node, whereas (9) corresponds to that with a variable node (or bit node) in the Tanner graph. The operation \boxplus of LLR is defined as [20]

$$L_a \boxplus L_b = \log \frac{1 + e^{L_a} e^{L_b}}{e^{L_a} + e^{L_b}} = 2 \tanh^{-1} \left(\tanh \left(\frac{L_a}{2} \right) \tanh \left(\frac{L_b}{2} \right) \right). \quad (10)$$

The recursive decoding procedure continues, starting from $k = n$ and until it reaches 1, where the last LLR on the right hand side of (6) and (7), i.e., $L_0^{(0)}(y_i)$, corresponds to the LLR of the channel bit x_i . For an AWGN channel, we have

$$L_0^{(0)}(y_i) = \log \frac{\Pr(y_i | x_i = 0)}{\Pr(y_i | x_i = 1)} = 4 \frac{\sqrt{E_s}}{N_0} y_i, \quad i = 0, 1, \dots, N - 1. \quad (11)$$

C. Polar Code Construction

For polar codes with rate $R = K/N$, K channels out of N total channels are selected for information transmission. Let $\mathcal{I} \subset \{0, 1, \dots, N-1\}$ denote the set of the channel indices selected to be information bits, i.e., the *information set* [1], with its cardinality given by $|\mathcal{I}| = K$. The bits that are not in this set are called *frozen bits* and fixed to known values (usually set as 0).

Therefore, polar code construction is equivalent to the selection of a set \mathcal{I} that leads to a good block error rate (BLER) performance.

In this work, we mostly focus on a Gaussian approximation (GA) based design of polar codes. This approach allows us to construct good polar codes with much less complexity than those based on precise density evolution. We demonstrate that the carefully designed GA will also be able to predict the achievable BLER performance by simulations for a given code with almost negligible computational effort.

III. IMPROVED GAUSSIAN APPROXIMATION

In this section, we first study the conventional GA approach, originally proposed for design and analysis of LDPC codes, and its limitations when applied to the design of polar codes. Then, through careful design of associated metric calculations, we show how to overcome these limitations by an improved GA.

A. Gaussian Approximation

Assume that the all-zero input sequence and thus the all-zero codeword is transmitted. Then, from (3) and (4), $y_i \sim \mathcal{N}(\sqrt{E_s}, N_0/2)$ for all i and thus from (11) we observe that $L_0^{(0)} \triangleq L_0^{(0)}(y_i) \sim \mathcal{N}(\gamma_0, 2\gamma_0)$ with $\gamma_0 = 4E_s/N_0$. We refer to the initial value of E_s/N_0 as the *design SNR* [9], [12], denoted by SNR_{des} , when this value is used for construction of polar codes. (Note that the design SNR is not given with respect to the conventional E_b/N_0 where E_b is defined as the energy *per information bit*, since E_b/N_0 is a function of E_s/N_0 and the code rate and thus is not convenient when comparing transmissions of codewords with the same symbol energy but different code rate.) From (8), (9), and (10) with the assumption that the previous bits are correctly estimated (i.e., $\hat{\mathbf{u}}_{i-1} = \mathbf{0}_i$ for a given i , where $\mathbf{0}_m$ denotes the zero vector of length m), we have

$$\tanh\left(\frac{L_k^{(2i)}}{2}\right) = \tanh\left(\frac{L_{k-1}^{(i)}}{2}\right) \tanh\left(\frac{L_{k-1}^{(i)'}}{2}\right), \quad (12)$$

$$L_k^{(2i+1)} = L_{k-1}^{(i)} + L_{k-1}^{(i)'}, \quad (13)$$

for $k = 1, 2, \dots, n$, and $i = 0, 1, \dots, 2^{k-1} - 1$ with $n = \log_2 N$, where both $L_{k-1}^{(i)}$ and $L_{k-1}^{(i)'}$ can be considered as independent and identical distributed (i.i.d.) random variables due to the structure

of the polar codes with SC decoding. Under the assumption that the LLRs $L_{k-1}^{(i)}$ and $L_{k-1}^{(i)'}$ follow a $\mathcal{N}(\gamma_{k-1}^{(i)}, 2\gamma_{k-1}^{(i)})$ distribution, the only parameter required to characterize its statistical distribution is its mean. In fact, if this Gaussian assumption holds, since the two LLRs on the right hand side of (13) are statistically independent, it follows from (13) that the output $L_k^{(2i+1)}$ should precisely follow $\mathcal{N}(2\gamma_{k-1}^{(i)}, 4\gamma_{k-1}^{(i)})$, i.e.,

$$\gamma_k^{(2i+1)} = 2\gamma_{k-1}^{(i)}. \quad (14)$$

On the other hand, the transformation (12) changes the statistical distribution of the output $L_k^{(2i)}$ from Gaussian. Nevertheless, Chung *et al.* applied statistical expectation to both sides of (12) to get [8]

$$\begin{aligned} E \left[\tanh \left(\frac{L_k^{(2i)}}{2} \right) \right] &= E \left[\tanh \left(\frac{L_{k-1}^{(i)}}{2} \right) \right] E \left[\tanh \left(\frac{L_{k-1}^{(i)'}}{2} \right) \right] \\ &= \left(E \left[\tanh \left(\frac{L_{k-1}^{(i)}}{2} \right) \right] \right)^2. \end{aligned} \quad (15)$$

Upon calculating (15), let us define the monotonically increasing function $\psi(\gamma) : (0, \infty) \rightarrow (0, 1)$ with respect to the mean γ of the random variable $L \sim \mathcal{N}(\gamma, 2\gamma)$ as

$$\psi(\gamma) = E \left[\tanh \left(\frac{L}{2} \right) \right] = \int_{-\infty}^{\infty} \tanh \left(\frac{x}{2} \right) \frac{1}{\sqrt{4\pi\gamma}} e^{-\frac{(x-\gamma)^2}{4\gamma}} dx. \quad (16)$$

Then, we may rewrite (15) as

$$\gamma_k^{(2i)} = \psi^{-1} \left(\psi^2 \left(\gamma_{k-1}^{(i)} \right) \right). \quad (17)$$

Note that the compound function $\psi^{-1}(\psi^2(\gamma)) : (0, \infty) \rightarrow (0, \infty)$ is monotonically increasing. However, since $\psi(\gamma)$ is strictly increasing in γ with $0 < \psi(\gamma) < 1$, we have $\psi^2(\gamma) < \psi(\gamma)$ and hence $\psi^{-1}(\psi^2(\gamma)) < \gamma$. Therefore, it always returns the output value that is strictly smaller than the input.

Instead of directly dealing with $\psi(\gamma)$, Chung *et al.* introduce its complement function

$$\phi(\gamma) = 1 - \psi(\gamma). \quad (18)$$

In this case, $\phi(\gamma)$ is a monotonically decreasing function and approaches zero as $\gamma \rightarrow \infty$, and (17) can be expressed as

$$\gamma_k^{(2i)} = \phi^{-1} \left(1 - \left(1 - \phi \left(\gamma_{k-1}^{(i)} \right) \right)^2 \right). \quad (19)$$

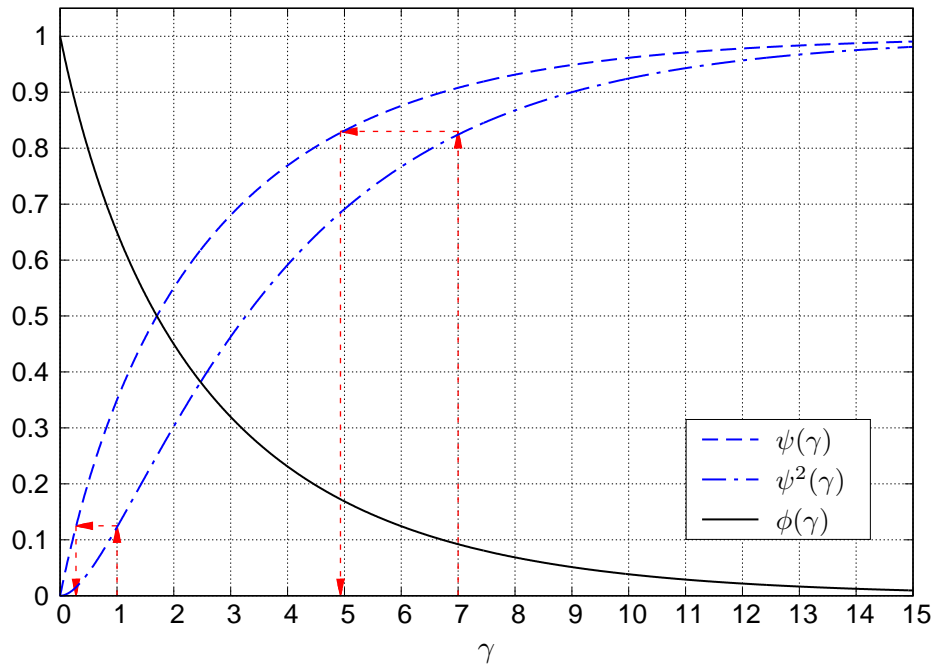


Fig. 1. The mean LLR converting functions $\psi(\gamma)$, $\phi(\gamma)$ and its associated function $\psi^2(\gamma)$. The trajectories demonstrate how the mean value is converted by the equation (17).

Fig. 1 plots the associated functions $\psi(\gamma)$, $\psi^2(\gamma)$, and $\phi(\gamma)$, which are calculated by numerical integration. The trajectories in the figure show how the mean value γ is converted by the transformation of (17), and it is apparent that this transformation always reduces the mean LLR value.

In [8], the approximation

$$\phi(\gamma) = e^{a\gamma^c + b} \quad (20)$$

was suggested for $\phi(\gamma)$ in (18) for the case that $\gamma < \gamma_{\text{th}}$ where γ_{th} is some threshold. Here, the constants were numerically determined as $a = -0.4527$, $b = 0.0218$, $c = 0.86$. For the case of $\gamma > \gamma_{\text{th}}$, based on the relationship

$$\sqrt{\frac{\pi}{\gamma}} e^{-\frac{\gamma}{4}} \left(1 - \frac{3}{\gamma}\right) < \phi(\gamma) < \sqrt{\frac{\pi}{\gamma}} e^{-\frac{\gamma}{4}} \left(1 + \frac{1}{7\gamma}\right), \quad (21)$$

and since the upper and lower bounds converge as $\gamma \rightarrow \infty$, it was suggested to approximate $\phi(\gamma)$ by the average of the upper and lower bounds in (21), i.e.,

$$\phi(\gamma) \approx \sqrt{\frac{\pi}{\gamma}} e^{-\frac{\gamma}{4}} \left(1 - \frac{10}{7\gamma}\right). \quad (22)$$

The threshold value was chosen to be $\gamma_{\text{th}} \approx 10$. For small γ , (20) may not be accurate as $\gamma \rightarrow 0$. Therefore, even if (20) may be sufficient for the moderate size of N as confirmed in [10], [11], the performance degradation may occur for large code length N due to numerical inaccuracy as is pointed out in [21].

There are two numerical computation issues with the above GA approach. The first issue is due to the approximation associated with (20) for a small value of γ , which results in $\lim_{\gamma \rightarrow 0} \phi(\gamma) = e^b > 1$. As a consequence, when γ approaches zero (i.e., once the mean LLR falls below a certain level), the input to the inverse function $\phi^{-1}(\cdot)$ of (19) fails to approach one and thus γ cannot become zero, rendering further polarization effects untraceable. The second issue is due to the fact that the function $\phi(\gamma)$ returns a value in the interval $(0, 1)$ and can thus approach arbitrarily close to zero as γ becomes large. For example, when $\gamma = 1000$, which is a typical value in the case of polar codes with relatively large code length, we observe that $\phi(\gamma) \approx 1.49 \times 10^{-110}$. Therefore, as γ becomes large (i.e., once the mean LLR exceeds a certain level), the inverse function $\phi^{-1}(\cdot)$ fails to return an accurate value, and thus again makes further polarization untraceable. These issues can be solved by the proposed log-domain calculation technique of the function $\phi(\gamma)$ described in what follows.

Remark: It is worth noting that even though the initial LLR of bit channels $L_0^{(0)}$ is Gaussian distributed, there is no guarantee that $L_k^{(2i)}$ can be treated as Gaussian, since the output after \boxplus operation, i.e., (8), is not strictly Gaussian. (This issue is discussed in detail in the APPENDIX.) However, the notable aspect associated with the use of (15) is that even if $L_k^{(2i)}$ is not Gaussian, the mean $\gamma_k^{(2i)}$ is chosen such that $L_k^{(2i)}$ is *approximated* by a Gaussian with mean $\gamma_k^{(2i)}$ and variance $2\gamma_k^{(2i)}$. Therefore, the computed $\gamma_k^{(2i)}$ will be different from a direct calculation of the LLR mean:

$$E \left[L_k^{(2i)} \right] = 2E \left[\tanh^{-1} \left\{ \tanh \left(\frac{L_{k-1}^{(i)}}{2} \right) \tanh \left(\frac{L_{k-1}^{(i)'}}{2} \right) \right\} \right]. \quad (23)$$

In the APPENDIX, we describe the theoretical derivation of the above mean value.

Fig. 2 compares the mean LLR of improved GA (based on the numerical algorithm described in the next subsection) and the mean LLR of (23), derived as (52) in the APPENDIX, for a given input mean LLR. From the figure, we observe that the behavior of the two functions are significantly different, especially as the mean input LLR increases. Due to this difference, the use of mean LLR directly calculated through (23) may not lead to the same result as the

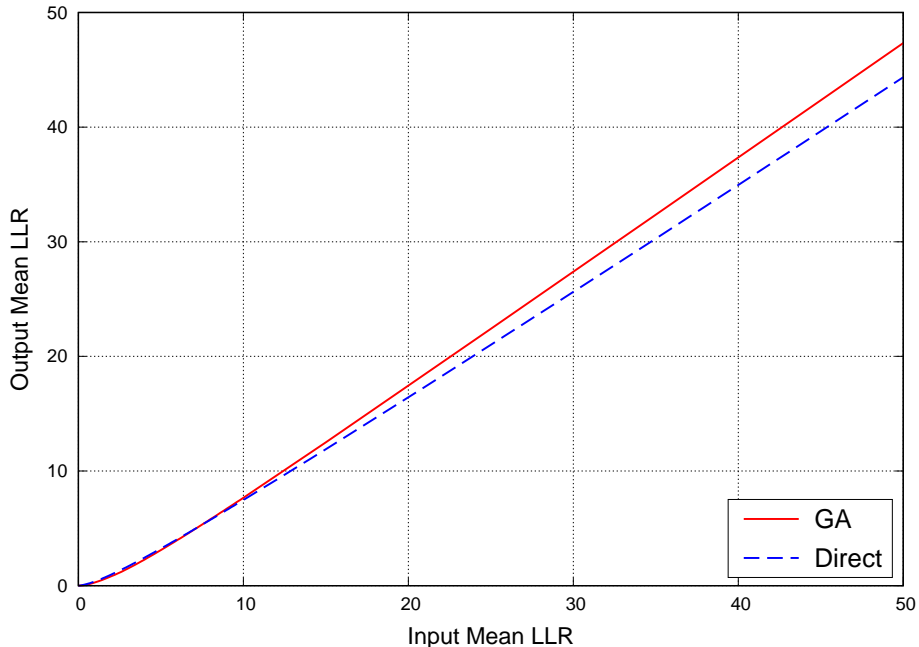


Fig. 2. Comparison of the output mean LLR values of \boxplus operation based on GA and direct calculation.

conventional GA approach through (15). In Section V, we will see that this *direct calculation* approach does not perform well when applied to polar code construction.

B. Log-Domain Function Approach for LLR Calculation of GA

In what follows, we describe a tractable approach for GA that is effective even in the case of large N . Recall that the mean LLR of polar codes at the code construction design stage should range from very small values to very large values, and the metric calculation associated with GA should support this exponential range. For example, if the design SNR is 1 (i.e., 0 dB), then the initial mean LLR value should be $\gamma_0 = 4$. For the polar code with $N = 2^n$, since each operation of (13) doubles the LLR value as shown in (14), the largest value (after n stages) is $L_{\max} = 4 \times 2^n$. On the other hand, the amount of change from γ_{k-1} to γ_k according to (12) depends on its input value, and as is observed from Fig. 1, its ratio γ_k/γ_{k-1} rapidly becomes smaller as γ_{k-1} decreases and the ratio becomes much less than $1/2$ with small enough γ_{k-1} . Therefore, in order to track the mean values by GA accurately, γ_k must be precisely calculated even if it becomes extremely small as discussed in the previous subsection. As N increases, and thus potentially better coding gain is achieved, we can expect that the operating SNR can be

decreased and thus the initial value γ_0 will also decrease. Therefore, unless GA can precisely trace the evolution of the mean value γ_k with high accuracy, the resulting codes may fail to achieve the polarization effect once it reaches some low LLR values.

To cope with this issue, we define the logarithmic domain of $\phi(\gamma)$ as

$$\xi(\gamma) = \log \phi(\gamma) = \log(1 - \psi(\gamma)) \quad (24)$$

such that we can accurately trace the mean LLR value even in the case with $\gamma \rightarrow 0$ or $\gamma \rightarrow \infty$. Note that $\xi(\gamma) : (0, \infty) \rightarrow (-\infty, 0)$, and $\xi(\gamma)$ is monotonically decreasing with γ . Therefore, tracking $\xi(\gamma)$ is equivalent to tracking $\phi(\gamma)$, and (19) can be rewritten with respect to $\xi(\gamma)$ as

$$\gamma_k^{(2i)} = \xi^{-1} \left(\xi \left(\gamma_{k-1}^{(i)} \right) + \log \left(2 - e^{\xi(\gamma_{k-1}^{(i)})} \right) \right) \quad (25)$$

whereas $\gamma_k^{(2i+1)}$ is revised according to (14). Two major advantages of using (24) are that i) as $\gamma \rightarrow 0$, $\xi(\gamma) \approx -\psi(\gamma)$ since $\psi(\gamma) \rightarrow 0$ as well, and thus $\xi(\gamma)$ can accurately trace γ in this regime as well (it will be shown below that $\xi(\gamma) \approx -\gamma/2$), and ii) for $\gamma \rightarrow \infty$, then $\psi(\gamma) \rightarrow 1$, and it will be shown that $\xi(\gamma)$ is, to the first order, linear in γ , and thus γ can again be accurately traced in this regime. By comparison, when γ is large, $\psi(\gamma) \approx 1$ (see Fig. 1), and $\psi(\gamma)$ would need to be computed with very high precision to obtain γ from its inverse as even a slight error in $\psi(\gamma)$ can result in an incorrect inverse γ .

The remaining issue is how to describe $\xi(\gamma)$ depending on the value of γ . Note that the inverse function of $\xi(\gamma)$ is required in (25) and thus the preferable form is such that its inverse can be described in a simple closed form.

1) *For Small Values of γ* : We first consider the case with $\gamma \rightarrow 0$. Noticing that $\lim_{\gamma \rightarrow 0^+} \psi'(\gamma) = 1/2$ and $\lim_{\gamma \rightarrow 0^+} \psi(\gamma) = 0$, we have

$$\lim_{\gamma \rightarrow 0^+} \frac{d\xi(\gamma)}{d\gamma} = \lim_{x \rightarrow 0^+} -\frac{\psi'(x)}{1 - \psi(x)} = -\frac{1}{2}, \quad (26)$$

leading to

$$\xi(\gamma) \approx -\frac{1}{2}\gamma. \quad (27)$$

2) *For Large Values of γ* : This asymptotic case was rigorously analyzed in [8]. Alternatively, by applying the identity $\tanh(x/2) = 1 - 2/(e^x + 1)$ to (16), we may rewrite (18) directly

through series expansion as

$$\begin{aligned}
\phi(\gamma) &= \frac{1}{\sqrt{\pi\gamma}} \int_{-\infty}^{\infty} \frac{1}{e^x + 1} e^{-\frac{(x-\gamma)^2}{4\gamma}} dx = \frac{e^{-\frac{\gamma}{4}}}{\sqrt{\pi\gamma}} \int_{-\infty}^{\infty} \frac{e^{\frac{x}{2}}}{e^x + 1} e^{-\frac{x^2}{4\gamma}} dx \\
&= \frac{e^{-\frac{\gamma}{4}}}{\sqrt{\pi\gamma}} \int_{-\infty}^{\infty} \frac{e^{\frac{x}{2}}}{e^x + 1} \sum_{k=0}^{\infty} \frac{1}{k!} \left(-\frac{x^2}{4\gamma}\right)^k dx = \frac{e^{-\frac{\gamma}{4}}}{\sqrt{\pi\gamma}} \sum_{k=0}^{\infty} \frac{(-1)^k}{k!(4\gamma)^k} \int_{-\infty}^{\infty} x^{2k} \frac{e^{\frac{x}{2}}}{e^x + 1} dx \\
&= \frac{e^{-\frac{\gamma}{4}}}{\sqrt{\pi\gamma}} \sum_{k=0}^{\infty} \frac{(-1)^k (2k)!}{(16\gamma)^k k!} \left\{ \zeta\left(2k+1, \frac{1}{4}\right) - \zeta\left(2k+1, \frac{3}{4}\right) \right\} \\
&= \frac{e^{-\frac{\gamma}{4}}}{\sqrt{\pi\gamma}} \left(\pi - \frac{\pi^3}{4\gamma} + \frac{5\pi^5}{32\gamma^2} - \frac{61\pi^7}{384\gamma^3} + \dots \right), \tag{28}
\end{aligned}$$

where $\zeta(m, q)$ is the generalized Riemann zeta function defined as

$$\zeta(m, q) = \sum_{l=0}^{\infty} \frac{1}{(l+q)^m}. \tag{29}$$

Listing the first two terms of the summation in (28) leads to the following approximate formula:

$$\phi(\gamma) \approx \sqrt{\frac{\pi}{\gamma}} e^{-\frac{\gamma}{4}} \left(1 - \kappa_0 \frac{\pi^2}{\gamma} \right), \tag{30}$$

where we have introduced a positive constant κ_0 as a fitting parameter that is to be determined numerically at some reference point of γ . It is clear that the impact of κ_0 becomes negligible as γ increases. (The expression (30) has the same asymptotic form as (22) for large γ as expected, but the constant κ_0 is kept for better accuracy.) Consequently, we have

$$\xi(\gamma) \approx -\frac{\gamma}{4} + \frac{1}{2} \log \pi - \frac{1}{2} \log \gamma + \log \left(1 - \kappa_0 \frac{\pi^2}{\gamma} \right). \tag{31}$$

3) *For Moderate Values of γ* : In this case, we may use a function that decreases monotonically as γ increases. We divide the entire range of interest into M regions and for $i = 1, \dots, M$, we propose to use the following form

$$\xi(\gamma) \approx -\alpha_i \gamma^{\beta_i}, \quad \text{for } \Gamma_i \leq \gamma < \Gamma_{i+1}, \tag{32}$$

where α_i and β_i are the parameters we numerically determine for a given interval $[\Gamma_i, \Gamma_{i+1})$. The above form is chosen for the convenience of computing its inverse function and ease of parameter fitting. More complex functions with better approximation may be possible, but the issue will not be pursued here.

TABLE I

THE PARAMETERS FOUND THROUGH NUMERICAL SEARCH.

| k | α_k | β_k | Γ_k | Z_k |
|-----|------------|-----------|------------|--------|
| 1 | 0.433 | 0.9303 | 0.13 | -0.065 |
| 2 | 0.437 | 0.8722 | 1.17 | -0.501 |
| 3 | - | - | 10.15 | -3.30 |

Based on the above procedure and through numerical optimization with $M = 2$, we get

$$\xi(\gamma) = \begin{cases} -\frac{1}{2}\gamma, & \gamma < \Gamma_1, \\ -\alpha_1\gamma^{-\beta_1}, & \Gamma_1 \leq \gamma < \Gamma_2, \\ -\alpha_2\gamma^{-\beta_2}, & \Gamma_2 \leq \gamma < \Gamma_3, \\ -\frac{\gamma}{4} + \frac{1}{2}\log\pi - \frac{1}{2}\log\gamma + \log\left(1 - \kappa_0\frac{\pi^2}{\gamma}\right), & \Gamma_3 \leq \gamma, \end{cases} \quad (33)$$

where best parameters found through exhaustive curve-fitting search are listed in Table I with $\kappa_0 = 0.169$. The corresponding approximate functions are compared in Fig. 3, which shows perfect agreement in the case of $\gamma \rightarrow 0$. While the accuracy of the function for the asymptotic case of $\gamma \rightarrow \infty$ is not clear from Fig. 3, convergence is guaranteed by the above derivation.

4) *Inverse Function*: Given (33), the inverse function can be expressed as

$$\xi^{-1}(z) = \begin{cases} -2z, & Z_1 < z, \\ (z/\alpha_1)^{1/\beta_1}, & Z_2 < z \leq Z_1, \\ (z/\alpha_2)^{1/\beta_2}, & Z_3 < z \leq Z_2, \end{cases} \quad (34)$$

where Z_i is the threshold of two functions, i.e., $Z_i = \xi(\Gamma_i)$, and also listed in Table I. In the case of $z \leq Z_3$, the inverse function corresponding to (31) may not be expressed in a closed form. However, it can be easily calculated with high precision accuracy by using the bisection method.

Finally, the improved GA algorithm is summarized in Algorithm 1.

C. Block Error Rate Estimation

As discussed in [5], [7], [10], once the distribution of LLRs is determined by density evolution or the GA method, its block error rate (BLER) based on SC decoding can also be estimated.

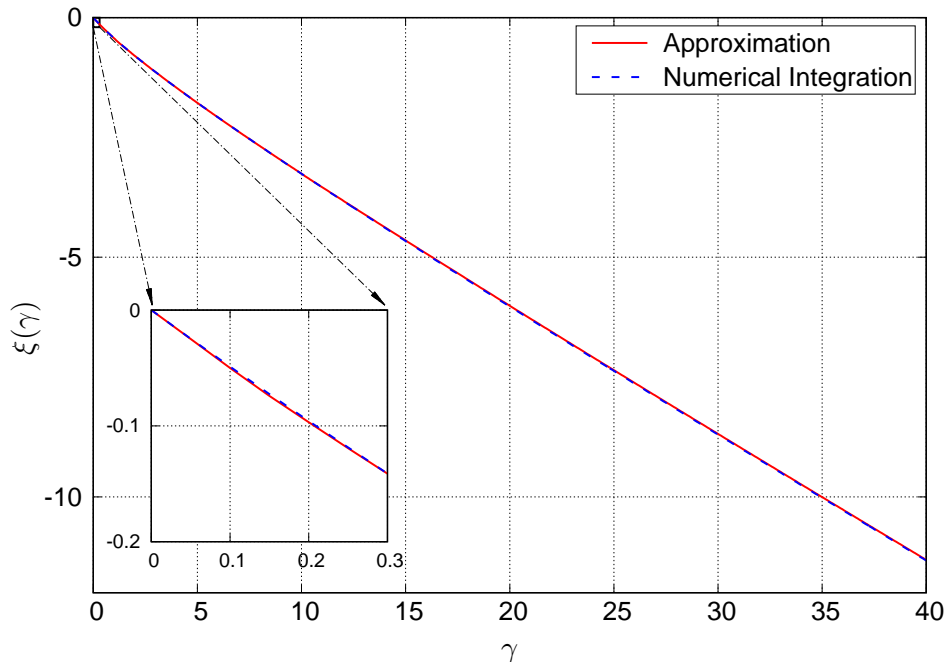


Fig. 3. Comparison of the function $\xi(\gamma)$ calculated through numerical integration and its approximate form (33). The area around the origin is zoomed up as a reference.

Assuming that the all zero codeword is transmitted, the bit error probability of the i th bit, provided that all the previous bits are correctly decoded, is given by

$$P_{b,i} = \Pr(\hat{u}_i \neq 0 | \hat{u}_0 = \dots = \hat{u}_{i-1} = 0) = \Pr(L_n^{(i)} < 0), \quad (35)$$

and under the assumption that $L_n^{(i)} \sim \mathcal{N}(\gamma_n^{(i)}, 2\gamma_n^{(i)})$, it follows that

$$P_{b,i} = Q\left(\sqrt{\frac{\gamma_n^{(i)}}{2}}\right), \quad (36)$$

where the Q -function $Q(x) : [0, \infty) \rightarrow (0, \frac{1}{2}]$ is defined as $Q(x) = \frac{1}{2}\text{erfc}\left(\frac{x}{\sqrt{2}}\right) = \frac{1}{\sqrt{2\pi}} \int_x^\infty e^{-\frac{t^2}{2}} dt$.

The BLER is expressed in general as

$$P_{BL} = 1 - \prod_{i=0}^{N-1} (1 - P_{b,i}), \quad (37)$$

and if we select a set of K channels with largest $\gamma_n^{(i)}$ as the information set \mathcal{I} , the minimum BLER with a given rate $R = K/N$ can be achieved. The resulting BLER is expressed as

$$P_{BL}(R, \text{SNR}_{\text{des}}) = 1 - \prod_{i \in \mathcal{I}} \left(1 - Q\left(\sqrt{\frac{\gamma_n^{(i)}}{2}}\right)\right), \quad (38)$$

Algorithm 1 Channel Polarization with Improved GA

Input: $n = \log_2 N$, SNR_{des}
Output: $\gamma[0], \gamma[1], \dots, \gamma[N-1]$ as $\gamma_n^{(0)}, \gamma_n^{(1)}, \dots, \gamma_n^{(N-1)}$

```

1:  $\gamma[0] = 4\text{SNR}_{\text{des}}$ 
2: for  $i = 1 : n$  do
3:    $J = 2^i$ 
4:   for  $j = 0 : J/2 - 1$  do
5:      $u = \gamma[j]$ 
6:      $z = \xi(u)$  using (33)
7:      $\gamma[j] = \xi^{-1}(z + \log(2 - e^z))$  using (34)
8:      $\gamma[j + J/2] = 2u$ 
9:   end for
10: end for
11: return  $\gamma[0], \gamma[1], \dots, \gamma[N-1]$ 

```

which can be interpreted as a function of the rate (since $R = |\mathcal{I}|/N$) and the design SNR (since $\gamma_0 = 4\text{SNR}_{\text{des}}$). By sorting $\gamma_n^{(i)}$ in a decreasing order (after applying the improved GA) before evaluation of (38) and selecting only the largest $|\mathcal{I}|$ elements from the entire index set $\{0, 1, \dots, N-1\}$, the best trade-off curve in terms of the code rate and BLER can be plotted for a given design SNR by sweeping the size $|\mathcal{I}|$ of the set \mathcal{I} .

As a consequence, if the mean LLR values of the bits in the information bit set \mathcal{I} are precisely calculated by GA, the resulting BLER by SC decoder for a given design SNR and code rate $R = K/N$ can be precisely estimated by (38), provided that the BLER is evaluated at the channel SNR that is equal to the design SNR.

Note that, as discussed in the APPENDIX, channels with large γ (i.e., good channels) can be well approximated by a Gaussian distribution through GA, whereas the channels with small γ (i.e., bad channels) may not be necessarily so. However, since in principle only the good channels are used for transmission and the statistical property of bad channels do not contribute to the calculation of BLER in (38), the performance of well designed polar codes that successfully select the good channels only may be closely characterized by (38).

IV. AN ALTERNATIVE CONSTRUCTION BASED ON LLR FLIPPING PROBABILITY

In the previous section, we discussed numerical issues associated with mean LLR calculation in the GA method, and how to cope with them. However, the non-linearity of \tanh does not strictly preserve the Gaussianity of the distribution of LLR. In this section, we consider an alternative approach that avoids the use of the \boxplus operation upon calculation of the metric associated with check nodes by only tracking the probability where the LLR value is reversed. We refer to this construction approach as the *LLR flipping probability construction*. The resulting equations can be implemented with much less elaboration than GA, but it still requires the assumption that the LLR is Gaussian distributed. Numerical results will also reveal that such an approach is still effective for constructing polar codes with moderate length. We recognize that the same approach described here was independently proposed by Tahir and Rupp in [22]. However, for the purpose of comparison as well as completeness, we describe this simple and tractable approach based on our own understanding.

A. LLR Flipping Expression of Check Node Operation

From the relationship of the check node given in (8), it is easy to observe that

$$\text{Event} \left[L_k^{(2i)} < 0 \right] = \text{Event} \left[\left(L_{k-1}^{(i)} < 0 \cap L_{k-1}^{(i)'} > 0 \right) \cup \left(L_{k-1}^{(i)} > 0 \cap L_{k-1}^{(i)'} < 0 \right) \right]. \quad (39)$$

Since the two events under the union operation in the right hand side of (39) are mutually exclusive, we may express

$$\begin{aligned} \Pr \left(L_k^{(2i)} < 0 \right) &= \Pr \left(L_{k-1}^{(i)} < 0 \cap L_{k-1}^{(i)'} > 0 \right) + \Pr \left(L_{k-1}^{(i)} > 0 \cap L_{k-1}^{(i)'} < 0 \right) \\ &= \Pr \left(L_{k-1}^{(i)} < 0 \right) \Pr \left(L_{k-1}^{(i)'} > 0 \right) + \Pr \left(L_{k-1}^{(i)} > 0 \right) \Pr \left(L_{k-1}^{(i)'} < 0 \right) \\ &= 2 \Pr \left(L_{k-1}^{(i)} < 0 \right) \left[1 - \Pr \left(L_{k-1}^{(i)} < 0 \right) \right] \end{aligned} \quad (40)$$

where the last two equalities stem from the fact that $L_{k-1}^{(i)}$ and $L_{k-1}^{(i)'}$ are i.i.d. The above equation shows that the flipping probability of the LLR output from the check node is given by that of the input LLR. Therefore, the evolution of LLR through the check node can be traced through (40) if its flipping probability is of interest. However, the LLR evaluation through the variable node, i.e., calculation of (9) cannot be performed through this approach unless we know the distribution of the input LLR. Therefore, analogous to GA we assume that input LLR is Gaussian distributed

with mean μ and variance σ^2 , i.e., $L_{k-1}^{(i)} \sim \mathcal{N}(\mu, \sigma^2)$. Then, it follows that $L_k^{(2i+1)} \sim \mathcal{N}(2\mu, 2\sigma^2)$ and therefore

$$\Pr\left(L_{k-1}^{(i)} < 0\right) = Q\left(\sqrt{\frac{\mu^2}{\sigma^2}}\right), \quad (41)$$

$$\Pr\left(L_k^{(2i+1)} < 0\right) = Q\left(\sqrt{\frac{2\mu^2}{\sigma^2}}\right). \quad (42)$$

Consequently, we may write

$$\Pr\left(L_k^{(2i+1)} < 0\right) = Q\left[\sqrt{2}Q^{-1}\left(\Pr\left(L_{k-1}^{(i)} < 0\right)\right)\right], \quad (43)$$

where $Q^{-1}(\cdot) : (0, \frac{1}{2}] \rightarrow [0, \infty)$ is the *inverse Q-function* with $Q^{-1}[Q(x)] = x$, which can be calculated numerically through the bisection method.

Note that since $L_0^{(0)} \sim \mathcal{N}(\gamma_0, 2\gamma_0)$, we have

$$\Pr\left(L_0^{(0)} < 0\right) = Q\left(\sqrt{\frac{\gamma_0}{2}}\right) = Q\left(\sqrt{\frac{2E_s}{N_0}}\right), \quad (44)$$

which is simply the bit error rate (BER) of uncoded BPSK as expected.

The channel polarization probability computation based on LLR flipping is summarized in Algorithm 2. Similar to (38) in the case of GA, the BLER can be estimated by

$$P_{BL}(R, \text{SNR}_{\text{des}}) = 1 - \prod_{i \in \mathcal{I}} (1 - \Pr(L_n^{(i)} < 0)) \quad (45)$$

and thus selecting the channel indices with the smallest flipping probabilities $\Pr(L_n^{(i)} < 0)$ may lead to the minimization of the resulting BLER.

B. Remarks

Since the function $Q(\cdot)$ returns a probability, it can rapidly approach 1/2 or 0 through the transformation of (40). To improve numerical stability, one may use a log-domain approach similar to the improved GA described in this paper. For simplicity, this issue will not be discussed further. The design based on the LLR flipping probability depends on how accurate the Gaussian modeling is, associated with (43). It should be mentioned that the output LLR after \boxplus operation is not Gaussian in general, and this is especially the case when the input mean LLR is small as discussed in the APPENDIX. Therefore, calculating the equivalent mean LLR value through the inverse Q-function shown in (43) may not be necessarily accurate and the error may accumulate

Algorithm 2 Channel Polarization with LLR Flipping Probability

Input: $n = \log_2 N$, SNR_{des}
Output: $p[0], p[1], \dots, p[N-1]$ as $\Pr(L_n^{(0)} < 0), \Pr(L_n^{(1)} < 0), \dots, \Pr(L_n^{(N-1)} < 0)$

```

1:  $p[0] = Q(\sqrt{2\text{SNR}_{\text{des}}})$ 
2: for  $i = 1 : \log_2 N$  do
3:    $J = 2^i$ 
4:   for  $j = 0 : J/2 - 1$  do
5:      $z = p[j]$ 
6:      $p[j] = 2z(1 - z)$ 
7:      $p[j + J/2] = Q[\sqrt{2}Q^{-1}(z)]$ 
8:   end for
9: end for
10: return  $p[0], p[1], \dots, p[N-1]$ 

```

as this process is repeated. If this part can be implemented with a more accurate model, the performance (both BLER estimation and actual simulation based on this construction) would be further improved.

V. CODE DESIGN EXAMPLE

In this section, we investigate the effectiveness of our results on code construction and achievable BLER through numerical calculations as well as Monte-Carlo simulations. Throughout all simulations, we employ the exact LLR calculation (i.e., all the terms of (46) instead of the min-sum approximation discussed in the APPENDIX).

A. Estimated Block Error Rate Achieved by Improved GA

We first evaluate the estimated BLER based on (38) using the improved GA as a function of design SNR, and the results are shown in Fig. 4 for various range of the code length N and code rate R^1 . (The corresponding theoretical limits by BPSK signaling are also plotted

¹The conventional GA method can obtain nearly identical estimated BLER results (or even better for large N cases). However, as observed in Section V-B, these estimates are not accurate.

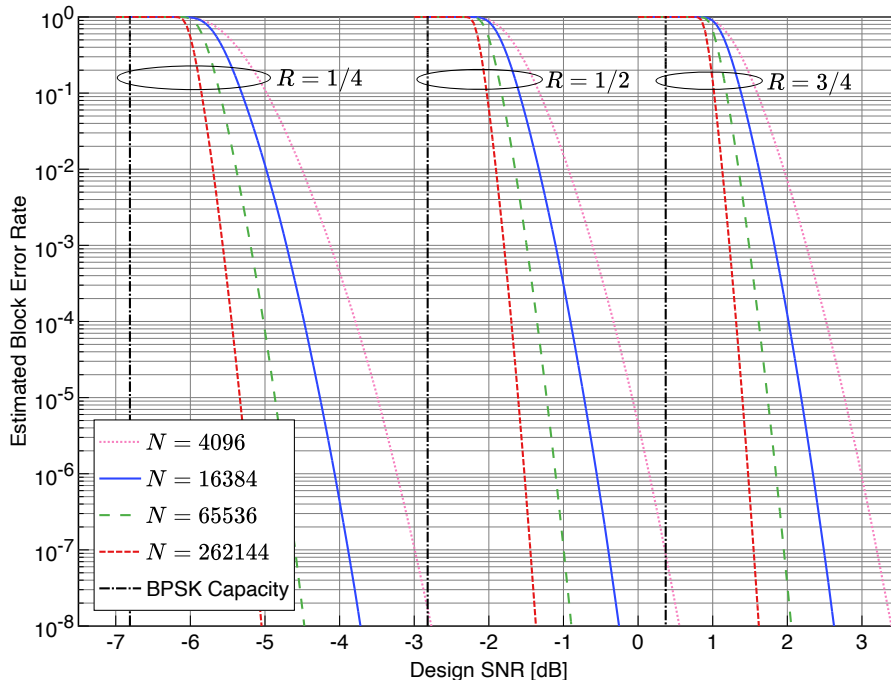


Fig. 4. Comparison of estimated BLER using the improved GA for given design SNR with various code length N and code rate R . The vertical lines indicate the minimum required E_s/N_0 in order to achieve the information rate by BPSK signaling (i.e., BPSK capacity). For each given design SNR, the code is constructed and the estimated BLER at a given target rate is calculated.

as vertical lines.) These BLER curves are plotted by applying improved GA for each design SNR, and then identifying the BLER using (38) for a given rate R . Therefore, each curve is the estimated performance when a code is designed at a specific SNR value and thus each curve is achieved by a *family* of polar codes with SC decoding, possibly with different information set at each SNR.

From Fig. 4, we observe that the gap between BLER curves and the corresponding capacity limits can be successfully reduced by increasing N , provided that the mean LLR is accurately estimated – Monte-Carlo simulations will show performance nearly identical to the estimate BLER curves.

B. Comparison with Conventional GA and Improved GA

We now compare the BLER performance of the conventional and improved GA through Monte-Carlo simulations and demonstrate how the conventional BLER diverges from the esti-

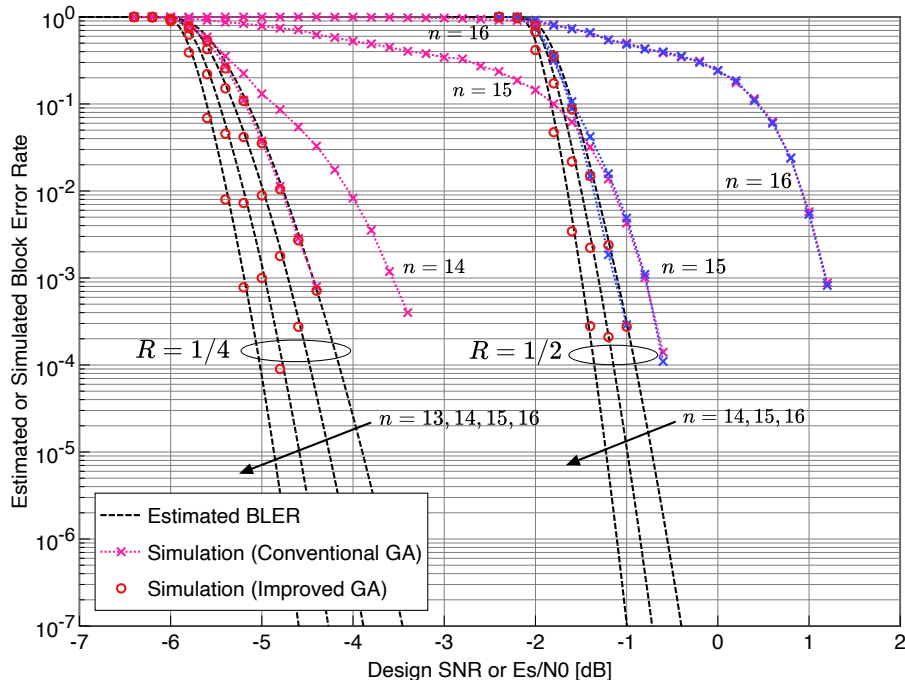


Fig. 5. Comparison of BLER for the conventional and improved GA where the simulated codes are constructed at the minimum design SNR where it achieves the estimated BLER of 10^{-3} . The code length is given by $N = 2^n$. The corresponding estimated BLER curve as a function of design SNR based on the improve GA is also plotted as a reference.

imated BLER as the code length increases. Fig. 5 shows the simulation results of polar codes of rate $1/2$ and rate $1/4$, constructed at the design SNR at which the estimated BLER of 10^{-3} can be achieved by (38). (How to select the design SNR for a given code rate will be further discussed in what follows.) The corresponding estimated BLER curves with respect to the design SNR, based on the improve GA, are also plotted as a reference. For the conventional GA, we apply (20) and (22), and the inverse function corresponding to (22) is calculated by the bisection method. The two code rate cases of $R = 1/2$ and $R = 1/4$ are evaluated with the code length ranging from $N = 2^{13} = 8192$ to $N = 2^{16} = 65536$. We observe that the polar codes constructed by the two GA perform almost identical up to some code length as expected, but start to diverge beyond $n = 14$, whereas the performance of the improved GA follows similar to the estimated BLER regardless of code length. It is also interesting to note that for the conventional GA with $n = 15$ and $n = 16$, the two BLER curves *with different code rate* eventually merge, which suggests that they share the same weak channels in the information set due to numerical inaccuracy of

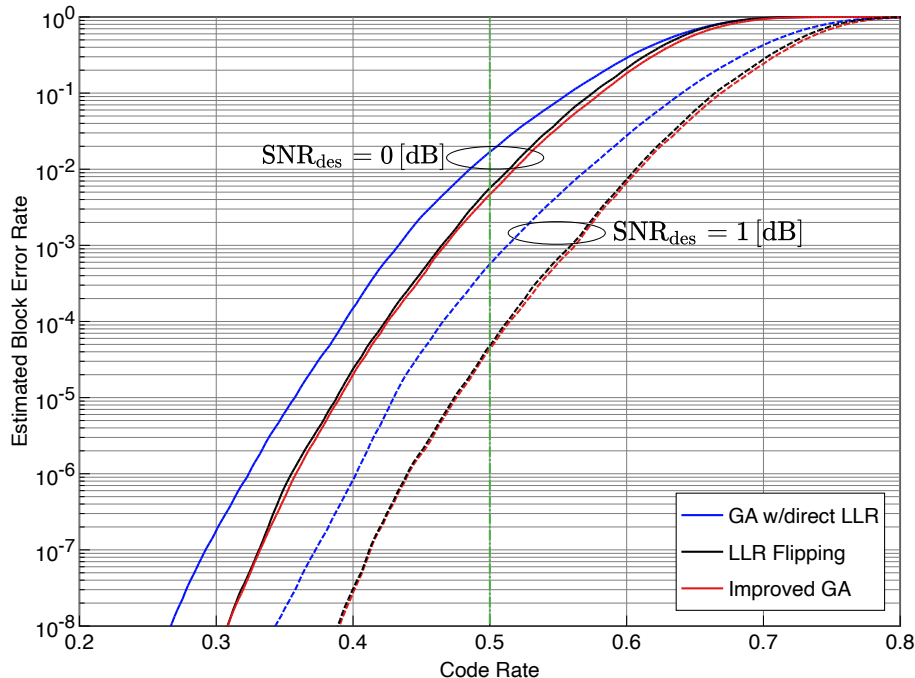


Fig. 6. Estimated BLER versus code rate for the specific polar codes constructed at design SNR of 0 dB and 1 dB. Three constructions are compared: improved GA, GA with direct mean LLR calculation, and LLR flipping probability.

the conventional GA, and this inaccuracy dominates the performance of SC decoding.

C. Comparison with Improved GA, Direct Approach, and LLR Flipping Probability

Next, we compare the performance of the construction based on the improved GA with the two other constructions: the GA with the mean LLR directly calculated from the output, and the construction based on the LLR flipping probability. Here, we take a relatively short code length of $N = 512$ as an example. (Note that for this short code length, the conventional GA has negligible numerical issues and the polar codes constructed by conventional and improved GA are identical.) Fig. 6 shows the estimated BLER and the achievable rate, which is calculated using (38) for the GA-based approach and using (45) for the LLR flipping probability approach. For each given design SNR, these BLER curves are calculated by selecting the K best channels, where K determined the achievable rate $R = K/N$. Two cases, one with design SNR of 0 dB and a second with design SNR of 1 dB are shown in the figure. Here, we observe that the estimated BLER by constructions based on the improved GA and the LLR flipping probability

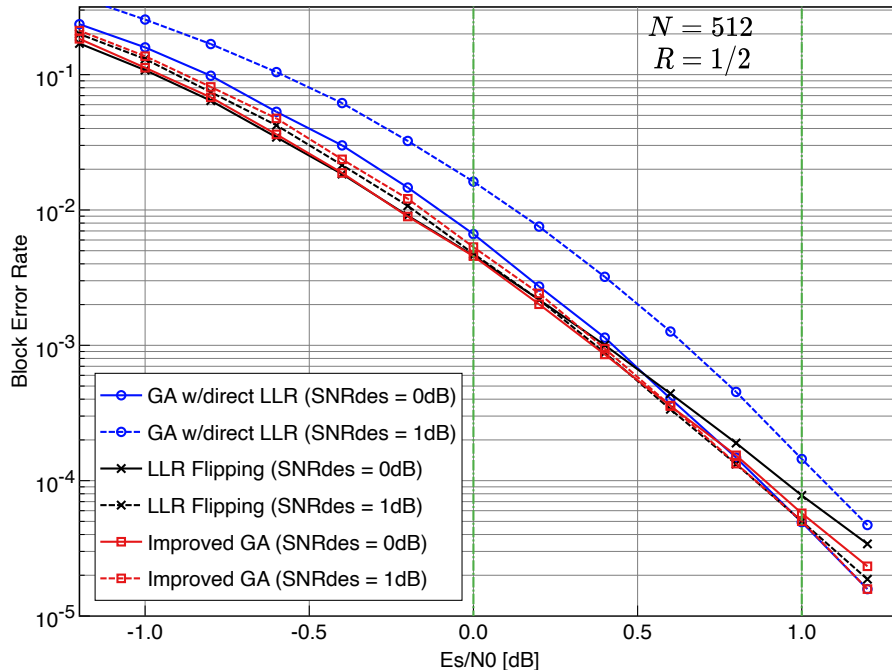


Fig. 7. BLER comparison of short polar codes (with $N = 512$) based on the three construction schemes designed with design SNR of 0 dB and 1 dB and code rate 1/2.

are similar, whereas the BLER based on the GA with direct LLR mean calculation shows noticeable degradation, which stems from the inaccuracy of the estimated LLR values.

Based on these observations, Fig. 7 shows the actual BLER curves of the rate-1/2 polar codes constructed with design SNR of 0 dB and 1 dB, evaluated through Monte-Carlo simulations. For each case, we observe that those based on the improved GA and LLR flipping probability show similar performance, whereas that based on the GA with direct LLR calculation shows some degradation. We also note that the former two schemes agree with the BLER estimated by Fig. 6 (i.e., the BLER values with rate 0.5 in Fig. 6 designed at SNR of 0 dB and 1 dB are almost the same as those in Fig. 7 observed at channel SNR of 0 dB and 1 dB, respectively), whereas the performance by the GA with direct LLR calculation is better than suggested by Fig. 6. From these results, it is clear that the GA based on the direct calculation of LLR mean is not suitable for BLER estimation as well as construction design, compared to the other two schemes.

D. Design Example of Improved GA for Large Code Length

Now, we consider the construction of polar codes with large code length. For the rest of this paper, we focus on the two cases: $N = 4096$ ($n = 12$) and $N = 262144$ ($n = 18$). Similar to Fig. 6, the estimated BLER results with respect to the code rate is shown in Fig. 8, where each design SNR is chosen as the minimum required SNR such that the estimated BLER of the improved GA reaches 10^{-3} for given rate of $1/2$ (0.5) and $3/4$ (0.75). For example, based on this code construction using the improved GA with $N = 4096$ and code rate $3/4$, the resulting code is expected to achieve a BLER of 10^{-3} at E_s/N_0 of 2.26 dB. We note that the construction based on the LLR flipping probability will be worse when the same parameter set up is selected, and the gap becomes noticeable as the code length increases. Therefore, it can be concluded that the construction based on the LLR flipping may not perform as good as that based on the improved GA, especially when the code length is large. It is conjectured that the main reason for this gap is due to the accumulation of the inaccuracy stemming from the Gaussian distribution approximations associated with variable node probability calculation. We therefore consider only the improved GA case in what follows.

Finally, Fig. 9 shows the BLER obtained by Monte-Carlo simulations, constructed based on the improved GA, where the associated parameters as well as the design SNR are chosen according to Fig. 8. The estimated BLER curves shown in the figure are taken from the corresponding results shown in Fig. 4. Recall that the polar codes are constructed such that they can achieve BLER of 10^{-3} at the design SNR, and from the figure we clearly observe that they behave as designed. We observe that when $n = 18$, the performance is well within 1 dB from the corresponding channel capacity at the BLER as low as 10^{-2} . Furthermore, the performance matches those of the estimated BLER curves constructed with each design SNR in the wide range of channel SNR (E_s/N_0). However, as the channel SNR increases, the simulated BLER is expected to diverge from the estimated BLER, which stems from the fact that the designed polar codes are not universal under SC decoding. If the target BLER is lower, the polar codes should be reconstructed with increasing design SNR.

We conclude this section by noting our observation that the simulated BLER becomes lower than the estimated BLER in low SNR regions. This may stem from the fact that in these regions, some channels in the information set \mathcal{I} may have low γ values. As discussed in the APPENDIX,

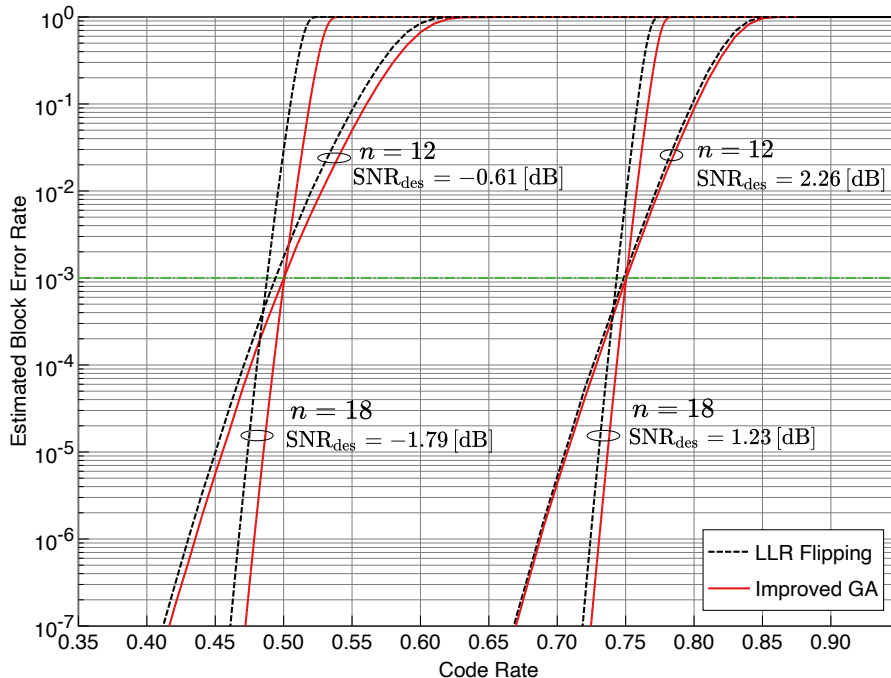


Fig. 8. Estimated BLER versus code rate for the specific polar codes constructed at the minimum design SNR where they achieve 10^{-3} of BLER measured at rate 1/2 or 3/4. Two constructions are compared: improved GA and LLR flipping probability.

the LLR values in the case of low γ deviates from the assumed Gaussian distribution of $\mathcal{N}(\gamma, 2\gamma)$, and thus the assumption of the error rate of bit channels by (36) becomes inaccurate (i.e., pessimistic).

VI. CONCLUSIONS

We have discussed a low-complexity approach to constructing polar codes with large code lengths based on an improved GA method assuming simple SC decoding. The estimated BLER shows the capacity approaching behavior as N increases, and the BLER obtained by the Monte-Carlo simulation with SC decoding matches this estimated BLER very well. Two other suboptimal approaches have been discussed and compared, showing the effectiveness of the improved GA. Finally, we note that the optimality of the construction based on GA is not yet proven, and there may exist polar codes that perform even better than the codes designed here. Furthermore, it is not clear if the codes designed here perform better with decoders other than SC, i.e., if they perform better with belief propagation (BP) and successive cancellation list (SCL) decoding at

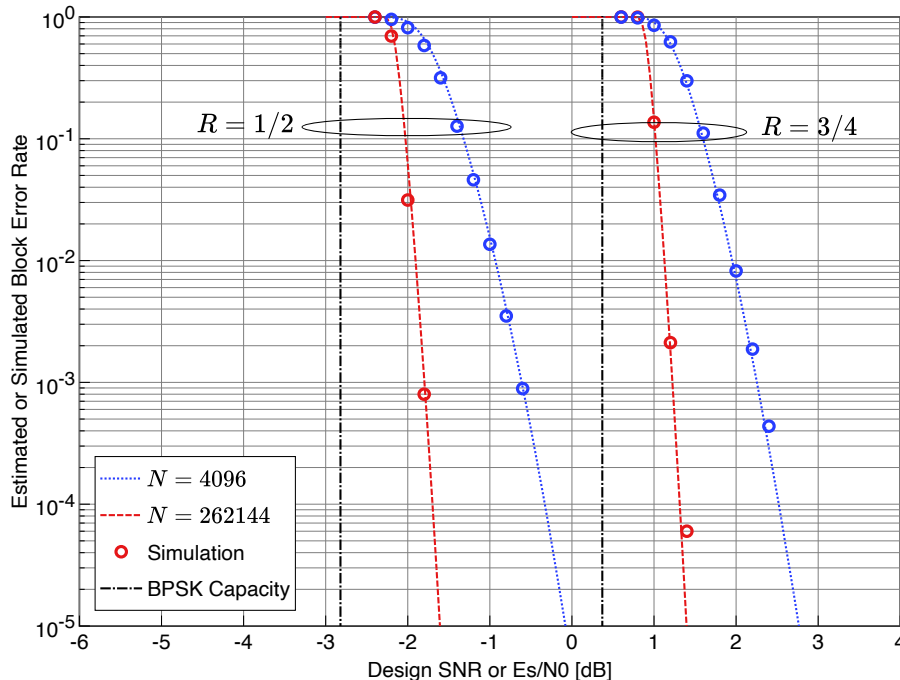


Fig. 9. Simulated and estimated BLER for the cases with $N = 4096$ ($n = 12$) and $N = 262144$ ($n = 18$). The simulated polar codes are constructed based on the improved GA with design SNR set at the minimum E_s/N_0 that achieves the estimated BLER of 10^{-3} as shown in Fig. 8. The corresponding BPSK capacity limits are also shown as vertical lines.

large code lengths. We leave this question for future work.

APPENDIX

In this appendix, we derive the mean value of the LLR output associated with the operation $L_o = L_a \boxplus L_b$, assuming that the two input LLRs L_a and L_b are independent Gaussian with $\mathcal{N}(\gamma, 2\gamma)$. We also discuss how the distribution of the output LLR converges to $\mathcal{N}(\gamma, 2\gamma)$ as γ increases based on the Kullback-Leibler (KL) divergence.

A. Mean of LLR Output

We first note that the output L_o associated with the \boxplus operation of two LLRs L_a and L_b can be expressed by the so-called min-sum form:

$$L_o \triangleq L_a \boxplus L_b \\ = \underbrace{\text{sign}(|L_a|) \text{sign}(|L_b|) \min(|L_a|, |L_b|)}_{\triangleq X} + \log(1 + e^{-|L_a+L_b|}) - \log(1 + e^{-|L_a-L_b|}), \quad (46)$$

where X corresponds to the output of the min-sum decoder, and is often used as a low-complexity alternative to exact decoding. As discussed in [23], based on the fundamental results on order statistics, the probability density function (pdf) of the random variable X defined above can be expressed as

$$f_X(x) = 2f_L(x) \{1 - F_L(|x|)\} + 2f_L(-x)F_L(-|x|), \quad (47)$$

where $f_L(x)$ and $F_L(x)$ are the pdf and cumulative distribution function (cdf) of L_a (or equivalently L_b), respectively. Assuming $L_a, L_b \sim \mathcal{N}(\gamma, 2\gamma)$, the above pdf can be expressed as

$$f_X(x) = \frac{1}{\sqrt{\pi\gamma}} \left\{ e^{-\frac{(x-\gamma)^2}{4\gamma}} Q\left(\frac{|x|-\gamma}{\sqrt{2\gamma}}\right) + e^{-\frac{(x+\gamma)^2}{4\gamma}} Q\left(\frac{|x|+\gamma}{\sqrt{2\gamma}}\right) \right\}. \quad (48)$$

Next, let us define the random variables $Y = |L_a + L_b|$ and $Z = |L_a - L_b|$ which appear in (46). Since $L_a + L_b \sim \mathcal{N}(2\gamma, 4\gamma)$ and $L_a - L_b \sim \mathcal{N}(0, 4\gamma)$, Y follows a *generalized Rice* distribution and Z follows a *generalized Rayleigh* distribution [24], whose pdfs are expressed as

$$f_Y(y) = \frac{1}{\sqrt{2\pi\gamma}} e^{-\frac{y^2+4\gamma^2}{8\gamma}} \cosh\left(\frac{y}{2}\right) \quad (49)$$

$$f_Z(z) = \frac{1}{\sqrt{2\pi\gamma}} e^{-\frac{z^2}{8\gamma}}. \quad (50)$$

Consequently, the mean of L_o can be expressed as

$$E[L_o] = E[X] + E[\log(1 + e^{-Y})] - E[\log(1 + e^{-Z})] \\ = \frac{1}{\sqrt{\pi\gamma}} \int_0^\infty \left[z e^{-\frac{(z-\gamma)^2}{4\gamma}} (1 - e^{-z}) \left[Q\left(\frac{z-\gamma}{\sqrt{2\gamma}}\right) - Q\left(\frac{z+\gamma}{\sqrt{2\gamma}}\right) \right] \right. \\ \left. - \frac{1}{\sqrt{2}} \log(1 + e^{-z}) \left\{ e^{-\frac{z^2}{8\gamma}} - \frac{1}{2} e^{-\frac{1}{8\gamma}(z-2\gamma)^2} (1 + e^{-z}) \right\} \right] dz \quad (51)$$

$$= \frac{1}{\sqrt{\pi}} \int_0^\infty \left[\sqrt{\gamma} x e^{-\frac{(x-\sqrt{\gamma})^2}{4}} (1 - e^{-\sqrt{\gamma}x}) \left[Q\left(\frac{x-\sqrt{\gamma}}{\sqrt{2}}\right) - Q\left(\frac{x+\sqrt{\gamma}}{\sqrt{2}}\right) \right] \right. \\ \left. - \frac{1}{\sqrt{2}} \log(1 + e^{-\sqrt{\gamma}x}) \left\{ e^{-\frac{x^2}{8}} - \frac{1}{2} e^{-\frac{1}{8}(x-2\sqrt{\gamma})^2} (1 + e^{-\sqrt{\gamma}x}) \right\} \right] dx, \quad (52)$$

where (52) may be convenient for small values of γ and (51) is suitable as γ increases for numerical evaluation.

B. KL Divergence Comparison

Our interest here is how the output LLR L_o with a given input mean LLR γ resembles the assumed Gaussian distribution $\mathcal{N}(\gamma_o, 2\gamma_o)$, where γ_o is the output mean LLR obtained by Gaussian approximation. To this end, we compare the Kullback-Leibler (KL) divergence between the two distributions. We note that the derivation of the exact distribution of L_o may be challenging, since the min-sum decoder output X is correlated with $Y = |L_a + L_b|$ and $Z = |L_a - L_b|$ in (46). Also, the effect of the two terms other than X in (46) is often small in practice. Therefore, we set X as our target distribution and we compare

$$D(f_X(x) \parallel \mathcal{N}(\gamma_o, 2\gamma_o)) = \int_{-\infty}^{\infty} f_X(x) \log \frac{f_X(x)}{g_X(x)} dx, \quad (53)$$

where

$$g_X(x) = \frac{1}{\sqrt{4\pi\gamma_o}} e^{-\frac{(x-\gamma_o)^2}{4\gamma_o}} \quad (54)$$

and the pdf $f_X(x)$ is derived in (48). Note that the parameter γ_o is obtained by (25) with γ as its input. Since $f_X(x)$ has the input mean LLR as a parameter γ , the above divergence can be uniquely determined for a given γ , and calculated by numerical integration.

The results are shown in Fig. 10, where we observe that the divergence rapidly decreases as γ increases. Since KL divergence is a measure of difference in two distributions and reaches 0 when they match perfectly, the smaller KL divergence indicates that $f_X(x)$ is closer to Gaussian with $\mathcal{N}(\gamma_o, 2\gamma_o)$. Therefore, the result in Fig. 10 convinces us that as the input mean LLR γ increases, the output may be approximated as $\mathcal{N}(\gamma_o, 2\gamma_o)$ as desired by GA. On the other hand, if γ is small, assuming the output LLR distribution as $\mathcal{N}(\gamma_o, 2\gamma_o)$ may exhibit inaccurate behavior. In the context of polar code construction, if the operating SNR is lower as in the case of low-rate code and thus the input mean LLR is likely to be small, then the trace of evolution by GA may not be necessarily accurate. Nevertheless, in the low code rate case in general, bad channels are not used, and thus the negative effect caused by this inaccuracy may be limited. Conversely, if the operating SNR is high as in the case of high-rate code, due to the accuracy of distribution approximation, GA is expected to accurately estimate the evolution of mean LLR, which leads

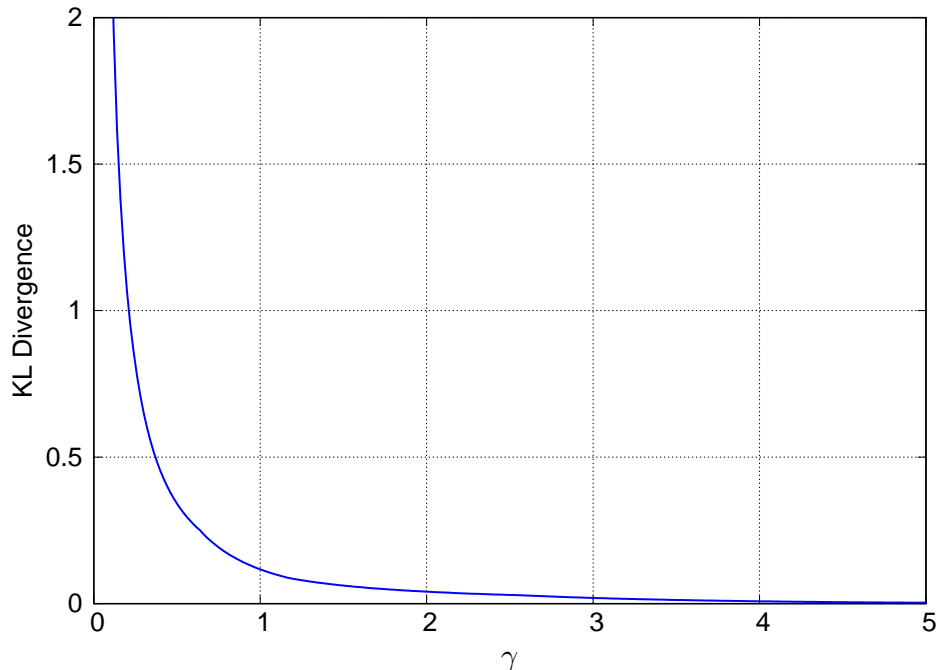


Fig. 10. KL divergence between the distribution of the min-sum function output and that assumed by GA.

to construction with better BLER estimation. In fact, in the results of Fig. 4, we observe that the polar codes constructed by GA with higher code rate exhibit performance much closer to the theoretical limit compared to the low code rate case which should begin GA process with the low γ value.

REFERENCES

- [1] E. Arıkan, “Channel polarization: A method for constructing capacity-achieving codes for symmetric binary-input memoryless channels,” *IEEE Trans. Inform. Theory*, vol. 55, pp. 3051–3073, 2009.
- [2] S. H. Hassani, S. B. Korada, and R. Urbanke, “The compound capacity of polar codes,” in *Proc. 2009 47th Ann. Allerton Conf. Commun., Contr., and Comput.*, pp. 16–21, Dec. 2009.
- [3] S. H. Hassani and R. Urbanke, “Universal polar codes,” in *Proc. 2014 IEEE Int. Symp. Inform. Theory (ISIT)*, pp. 1451–1455, June 2014.
- [4] E. Sasoglu and L. Wang, “Universal polarization,” *IEEE Trans. Inform. Theory*, vol. 62, pp. 2937–2946, June 2016.
- [5] R. Mori and T. Tanaka, “Performance of polar codes with the construction using density evolution,” *IEEE Commun. Lett.*, vol. 13, pp. 519–521, July 2009.
- [6] T. Richardson, M. A. Shokrollahi, and R. Urbanke, “Design of capacity-approaching irregular low-density parity-check codes,” *IEEE Trans. Inform. Theory*, vol. 47, pp. 619–637, Feb. 2001.
- [7] I. Tal and A. Vardy, “How to construct polar codes,” *IEEE Trans. Inform. Theory*, vol. 59, pp. 6562–6582, Oct. 2013.

- [8] S.-Y. Chung, T. Richardson, and R. Urbanke, "Analysis of sum-product decoding of low-density parity-check codes using a Gaussian approximation," *IEEE Trans. Inform. Theory*, vol. 47, pp. 657–670, Feb. 2001.
- [9] P. Trifonov, "Efficient design and decoding of polar codes," *IEEE Trans. Commun.*, vol. 60, pp. 3221–3227, Nov. 2012.
- [10] D. Wu, Y. Li, and Y. Sun, "Construction and block error rate analysis of polar codes over AWGN channel based on Gaussian approximation," *IEEE Commun. Lett.*, vol. 18, pp. 1099–1102, July 2014.
- [11] H. Li and J. Yuan, "A practical construction method for polar codes in AWGN channels," in *Proc. IEEE 2013 Tencon - Spring*, pp. 223–226, Apr. 2013.
- [12] H. Vangala, E. Viterbo, and Y. Hong, "A comparative study of polar code constructions for the AWGN channel." available on arXiv:1501.02473v1 [sc.IT], Jan. 2015.
- [13] S. B. Korada, A. Montanari, E. Telatar, and R. Urbanke, "An empirical scaling law for polar codes," in *Proc. 2010 IEEE Int. Symp. Inform. Theory (ISIT)*, pp. 884–888, June 2010.
- [14] E. Arıkan, "A performance comparison of polar codes and reed-muller codes," *IEEE Commun. Lett.*, vol. 12, pp. 447–449, June 2008.
- [15] N. Hussami, S. B. Korada, and R. Urbanke, "Performance of polar codes for channel and source coding," in *Proc. 2009 IEEE Int. Symp. Inform. Theory (ISIT)*, 2009.
- [16] A. Eslami and H. Pishro-Nik, "On finite-length performance of polar codes: Stopping sets, error floor, and concatenated design," *IEEE Trans. Commun.*, vol. 61, pp. 919–929, Mar. 2013.
- [17] I. Tal and A. Vardy, "List decoding of polar codes," *IEEE Trans. Inform. Theory*, vol. 61, pp. 2213–2226, May 2015.
- [18] M. Qin, J. Guo, A. Bhatia, A. G. i. Fabregas, and P. H. Siegel, "Polar code constructions based on LLR evolution," *IEEE Commun. Lett.*, vol. 21, pp. 1221–1224, June 2017.
- [19] A. Elkelesh, M. Ebada, S. Cammerer, and S. ten Brink, "Decoder-tailored polar code design using the genetic algorithm," *IEEE Trans. Commun.*, vol. 67, pp. 4521–4534, July 2019.
- [20] J. Hagenauer, E. Offer, and L. Papke, "Iterative decoding of binary block and convolutional codes," *IEEE Trans. Inform. Theory*, vol. 42, pp. 429–445, Mar. 1996.
- [21] J. Dai, K. Niu, Z. Si, C. Dong, and J. Lin, "Does Gaussian approximation work well for the long-length polar code construction?," *IEEE Access*, vol. 5, pp. 7950–7963, Jan. 2017.
- [22] B. Tahir and M. Rupp, "New construction and performance analysis of polar codes over AWGN channels," in *Proc. 24th Int. Conf. Telecommun. (ICT)*, pp. 1–4, May 2017.
- [23] D. Kern, S. Vorkoper, and V. Kühn, "A new code construction for polar codes using min-sum density," in *Proc. 8th Int. Symp. Turbo Codes & Iter. Inform. Process. (ISTC)*, pp. 228–232, June 2014.
- [24] J. G. Proakis and M. Salehi, *Digital Communications*. McGraw-Hill, fifth ed., 2008.